1

Nuclear Magnetic Resonance

1.1 Protons in a Magnetic Field

^{1}H-Nuclear magnetic resonance (NMR) is based on the manipulation of the magnetic moments of hydrogen nuclei (protons) in a strong magnetic field. A static magnetic field, $\mathbf{B}_0$, typically with a field strength of 1.5 or 3 T in clinical magnetic resonance imaging (MRI) scanners, induces macroscopic magnetization in the proton population inside a given object. Microscopically, $\mathbf{B}_0$ defines a quantization axis for the proton spin $\mathbf{S}$. Henceforth, we assume that $\mathbf{B}_0$ is aligned with the z-axis of the coordinate system: $\mathbf{B}_0 = (0, 0, B_0)^{\mathrm{T}}$. The proton has a spin quantum number $S = \frac{1}{2}$, meaning that $|\mathbf{S}| = \sqrt{S(S+1)}\hbar = \sqrt{\frac{3}{4}}\hbar$. Projection of $\mathbf{S}$ onto $\mathbf{B}_0$ can assume one of two possible values, $S_z = \pm\frac{1}{2}\hbar$, whereas the x- and y-components of the spin, S_x and S_y, according to the quantum mechanical uncertainty principle, remain undetermined. The proton spin is associated with a magnetic moment

$$\boldsymbol{\mu} = \gamma \mathbf{S}, \tag{1.1}$$

with the *gyromagnetic ratio* $\gamma = 2\pi \cdot 42.58\,\mathrm{MHz/T}$ for protons [7]. Thus, the z-component of the magnetic moment can assume either of two values

$$\mu_z = \pm\frac{1}{2}\gamma\hbar, \tag{1.2}$$

while μ_x and μ_y form an arbitrary and undetermined transverse magnetization component in the xy-plane. For each of the two possible values of μ_z, the potential energy of the respective state is

$$E = -\mathbf{B}_0 \bullet \boldsymbol{\mu} = -B_0 \cdot \mu_z, \tag{1.3}$$

indicating that the parallel alignment ($\uparrow\uparrow$) of μ_z with $\mathbf{B}_0$ has lower energy than the antiparallel ($\uparrow\downarrow$) orientation[1] [8]. The energy gap between the two states is therefore

$$\delta E = E_{\uparrow\downarrow} - E_{\uparrow\uparrow} = 2 \cdot B_0 \cdot \mu_z = \gamma \cdot B_0 \cdot \hbar. \tag{1.4}$$

1 Note that the sign conventions are somewhat misleading. For a magnetic field, the **B**-vector points from the north pole to the south pole. However, a magnetic dipole vector $\boldsymbol{\mu}$ points from the south pole to the north pole. The antiparallel orientation therefore means that the north poles of the field and the dipole are aligned, creating a repulsive torque that tries to flip the dipole by 180°, which explains why the antiparallel state possesses a higher potential energy than the parallel state.

Magnetic Resonance Elastography: Physical Background and Medical Applications, First Edition.
Sebastian Hirsch, Jürgen Braun, and Ingolf Sack.

Since protons are fermions, the distribution of the entire population of N protons over these two states is governed by a Fermi statistics [9]:

$$N_{\uparrow\uparrow} = N \cdot \frac{e^{-E_{\uparrow\uparrow}/k_B T}}{e^{-E_{\uparrow\uparrow}/k_B T} + e^{-E_{\uparrow\downarrow}/k_B T}} \tag{1.5}$$

$$N_{\uparrow\downarrow} = N \cdot \frac{e^{-E_{\uparrow\downarrow}/k_B T}}{e^{-E_{\uparrow\uparrow}/k_B T} + e^{-E_{\uparrow\downarrow}/k_B T}}. \tag{1.6}$$

The magnetic moments of protons in the parallel and antiparallel states cancel each other out. However, at human body temperature of 37 °C, the parallel, lower energy state has a slightly larger population than the excited antiparallel state. The excess population, with respect to the total population,

$$\delta N = \frac{N_{\uparrow\uparrow} - N_{\uparrow\downarrow}}{N} = \frac{e^{-E_{\uparrow\uparrow}/k_B T} - e^{-E_{\uparrow\downarrow}/k_B T}}{e^{-E_{\uparrow\uparrow}/k_B T} + e^{-E_{\uparrow\downarrow}/k_B T}}$$

is in the order of 10^{-6} at typical field strengths of clinical MRI scanners of 1.5 T or 3 T. This imbalance causes a small net magnetization

$$\mathbf{M}_0 = \delta N \rho |\mu_z| \hat{\mathbf{z}}, \tag{1.7}$$

with average proton density ρ and the unit vector $\hat{\mathbf{z}}$ along the z-axis. $\mathbf{M}_0$ is aligned with the static $\mathbf{B}_0$ field. Manipulation of this magnetization by means of additional time-dependent magnetic fields is the basis for all types of MR experiments. Despite the quantum mechanical nature of individual protons, the macroscopic magnetization can be treated in a classical way, since individual protons are never probed in MR imaging [9]. For a single proton, the transverse component of the magnetic moment (i.e., the projection of $\boldsymbol{\mu}$ onto the xy-plane) would have to be taken into account. However, by averaging over a large number of protons (in the order of Avogadro's constant, $N_A \approx 6 \cdot 10^{23}$), these contributions cancel each other out, so that no net transverse magnetization is observed in the equilibrium state.

1.2 Precession of Magnetization

For an arbitrary orientation of magnetization $\mathbf{M}$ with respect to the direction of $\mathbf{B}_0$, the time evolution of $\mathbf{M}$ is characterized by [10]:

$$\frac{\partial \mathbf{M}}{\partial t} = \gamma \mathbf{M} \times \mathbf{B}_0. \tag{1.8}$$

Total magnetization $\mathbf{M}(t)$ can be decomposed into a longitudinal component $\mathbf{M}_\parallel(t) = M_\parallel(t) \cdot \hat{\mathbf{z}}$ and a transverse component $\mathbf{M}_\perp(t)$ so that

$$\mathbf{M}(t) = \mathbf{M}_\parallel(t) + \mathbf{M}_\perp(t). \tag{1.9}$$

This allows us to separate Eq. (1.8) into

$$\frac{\partial \mathbf{M}_\parallel}{\partial t} = \gamma \mathbf{M}_\parallel \times \mathbf{B}_0 = \mathbf{0} \tag{1.10}$$

$$\frac{\partial \mathbf{M}_\perp}{\partial t} = \gamma \mathbf{M}_\perp \times \mathbf{B}_0. \tag{1.11}$$

Equation (1.11) describes the precession of the transverse magnetization about the axis defined by $\mathbf{B}_0$. The angular frequency of precession in a magnetic field of strength B is $\omega = \gamma B$, corresponding to the energetic separation $\delta E = \gamma B \hbar$ of the two states of μ_z of a single spin. If the magnetic field is solely determined by the static field $\mathbf{B}_0$, all magnetization precesses at the same frequency ω_0, which is also called *Larmor frequency*. In the presence of additional magnetic fields, $\mathbf{B} = \mathbf{B}_0 + \delta\mathbf{B}$, Eq. (1.8) becomes

$$\frac{\partial \mathbf{M}}{\partial t} = \gamma \mathbf{M} \times (\mathbf{B}_0 + \delta\mathbf{B}) \tag{1.12}$$

$$= \gamma \mathbf{M}_\perp \times \mathbf{B}_0 + \gamma \mathbf{M} \times \delta\mathbf{B}. \tag{1.13}$$

The right-hand side of Eq. (1.13) is a superposition of the previously mentioned precession of transverse magnetization and a rotation of full magnetization $\mathbf{M}$ about the axis defined by the arbitrary field vector $\delta\mathbf{B}$. In order to simplify the description, a coordinate transform can be performed from the static laboratory system to a reference frame (designated by primed symbols, e.g., $\mathbf{M}'$) that rotates about the z-axis with the Larmor frequency ω_0. Since this system rotates in synchrony with $\mathbf{M}_\perp$, transverse magnetization appears static and the first precession term in Eq. (1.13) vanishes. If $\delta\mathbf{B}$ is designed to rotate at the Larmor frequency in the transverse plane and to be aligned with the x'-axis, $\delta\mathbf{B}' = \mathbf{B}_1' = B_1 \cdot \hat{\mathbf{x}}'$, the rotating-frame version of Eq. (1.13) can be formulated as

$$\frac{\partial \mathbf{M}'}{\partial t} = \gamma B_1 \, (\mathbf{M}' \times \hat{\mathbf{x}}'), \tag{1.14}$$

or alternatively for a flip around the y'-axis:

$$\frac{\partial \mathbf{M}'}{\partial t} = \gamma B_1 \, (\mathbf{M}' \times \hat{\mathbf{y}}'). \tag{1.15}$$

In general, for an arbitrary vector $\boldsymbol{\omega}' = (\omega_1', \omega_2', \omega_3')^{\mathrm{T}} = \gamma \mathbf{B}'$, the motion of the magnetization is given by

$$\frac{\partial \mathbf{M}'}{\partial t} = (\mathbf{M}' \times \boldsymbol{\omega}'). \tag{1.16}$$

Figure 1.1 illustrates how such a $\mathbf{B}_1$-field can tilt the longitudinal magnetization from its initial equilibrium state into the transverse plane. Since the rotation frequency of the magnetization about the direction of $\mathbf{B}_1'$ is given by $\omega_{\mathrm{F}} = \gamma B_1'$, the flip angle[2] can be calculated as $\alpha(t) = \omega_{\mathrm{F}} \cdot t = \gamma B_1' \cdot t$. Arbitrary flip angles can thus be achieved by suitable combinations of B_1 field strength and the duration for which the field is switched on. Figure 1.1 illustrates the special case with $\alpha = 90°$.

A numerical method to simulate spin behavior under different kinds of applied magnetic fields is described in Appendix A.

1.2.1 Quadrature Detection

A precessing transverse magnetization induces a sinusoidal voltage signal $S(t) = S_0 \cdot \sin((\omega_0 + \delta\omega)t) \cdot \exp\left(-\frac{t}{T_{\mathrm{decay}}}\right)$ in a conductor loop (usually referred to as a *receive coil*), as shown in Figure 1.2. $\delta\omega$ denotes a small offset from ω_0 due to additional magnetic

2 "Flip angle" always refers to the angle by which a $\mathbf{B}_1$-pulse tilts the magnetization away from the direction of $\mathbf{B}_0$. The subscript "F" in ω_{F} refers to "flip."

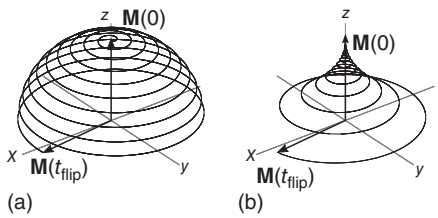

Figure 1.1 Time evolution of magnetization as seen from the laboratory frame. The black line traces the tip of $\mathbf{M}(t)$ over time. (a) During a 90°-pulse, the longitudinal equilibrium magnetization is tipped toward the transverse plane. The combination of precession at Larmor frequency and the tipping induced by the B_1 pulse causes the magnetization to spiral on a spherical shell from the z-axis toward the xy-plane. (b) After the B_1 pulse, the magnetization precesses at Larmor frequency. The transverse component of $\mathbf{M}$ decays with time constant T_2^*, whereas the longitudinal component relaxes back toward the equilibrium value $\mathbf{M}(0)$ with time constant T_1 (see Section 1.3).

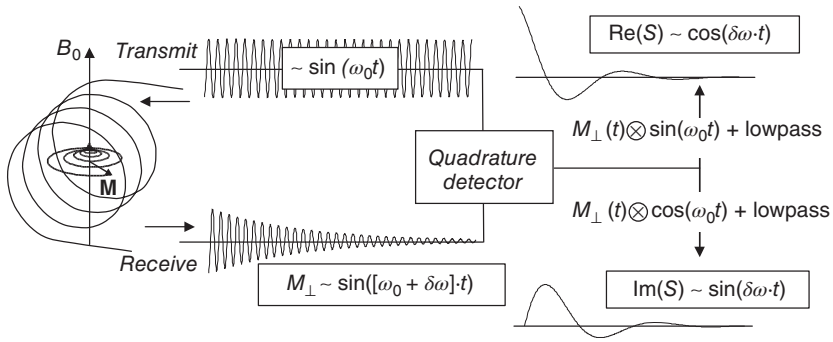

Figure 1.2 Illustration of the quadrature detection step of the MR signal acquisition. Details are explained in the text.

fields. The signal decay time constant[3] is either T_2 or T_2^*, depending on the type of echo (spin echo vs gradient echo, see Sections 1.5.1 and 1.5.2). The Larmor frequency ω_0 is irrelevant, and the desired information is only contained in the offset frequency $\delta\omega$ (see Section 1.6.1). In order to isolate $\delta\omega$, *quadrature detection* [11, pg. 371] is deployed.

Through quadrature detection, the received signal is divided into two branches and each is multiplied by either $\cos(\omega_0 t)$ or $\sin(\omega_0 t)$. Because of the trigonometric relations

$$\sin\alpha \cdot \sin\beta = \frac{1}{2}\left(\cos(\alpha-\beta) - \cos(\alpha+\beta)\right) \tag{1.17}$$

and

$$\sin\alpha \cdot \cos\beta = \frac{1}{2}(\sin(\alpha-\beta) + \sin(\alpha+\beta)) \tag{1.18}$$

the product signal is a sum of two signals, one oscillating with $\delta\omega$ and the other with $2\omega_0 + \delta\omega$. Since $\delta\omega \ll \omega_0$, a suitable low-pass filter will block the high frequency signal, so that the slow component $\delta\omega$ is obtained. The two filtered signals (from the sine and cosine branch) represent the real and imaginary parts of S. The conversion to magnitude

3 The different types of signal relaxation and their sources will be discussed in Section 1.3.

and phase can then be performed according to

$$|S| = \sqrt{|\mathrm{Re}(S)|^2 + |\mathrm{Im}(S)|^2} \tag{1.19}$$

$$\phi = \arctan\left(\frac{\mathrm{Im}(S)}{\mathrm{Re}(S)}\right). \tag{1.20}$$

The signal magnitude is proportional to the magnitude of transverse magnetization $|\mathbf{M}_\perp|$, and the phase ϕ is the angle between $\mathbf{M}_\perp$ and the x'-axis of the rotating frame.

1.3 Relaxation

The above discussion of precessing magnetization did not take dissipative interaction between spins and their environment into account. Since the parallel and antiparallel orientation of a magnetic moment with respect to $\mathbf{B}_0$ differ by energy $\delta E = \gamma \hbar B_0$, the interaction of a spin with its surroundings can change the orientation of its magnetic moment. This effect gives rise to *relaxation effects*, which are crucial for MRI signal and contrast generation.

In the thermal equilibrium state, the resultant magnetization $\mathbf{M}_0$ is aligned with $\mathbf{B}_0$, which defines the z-axis of the coordinate system. At any time point t, the total magnetization $\mathbf{M}(t)$ can be decomposed into longitudinal and transverse component, as introduced in Eq. (1.9). The presence of transverse magnetization indicates a perturbation of the equilibrium state. Through interaction with the microscopic lattice of the medium, excess energy is dissipated over time, so that the magnetization relaxes to the initial longitudinal state. The rate of change of the longitudinal magnetization component is proportional to its deviation from the equilibrium state:

$$\frac{\partial \mathbf{M}_\parallel}{\partial t} = \frac{1}{T_1}(\mathbf{M}_0 - \mathbf{M}_\parallel). \tag{1.21}$$

T_1 is the time constant of this relaxation process. It is dependent on the magnetic field strength and material properties. The range of T_1 in the human body at 37 °C and $B_0 = 1.5$ T ranges from 50 (muscle) to 4500 ms (cerebrospinal fluid) [10].

Thus far, spins have been treated as noninteracting particles. This is a rough approximation, since every spin is exposed to not only the external magnetic field but also the magnetic moments of its immediate surroundings. These interactions overlay with $\mathbf{B}_0$, so that every spin experiences a magnetic field as a sum of those two contributions. Hence, if the field strength is variable in space, $B = B(\mathbf{r})$, ω will also become position-dependent. This implies that magnetization vectors precessing at different locations will dephase over time, thus diminishing the resultant transverse magnetization. This effect is characterized by a first-order differential equation

$$\frac{\partial \mathbf{M}_\perp}{\partial t} = -\frac{1}{T_2}\mathbf{M}_\perp, \tag{1.22}$$

which is solved by a real-valued exponential function

$$\mathbf{M}_\perp(t) = \mathbf{M}_\perp(0) \cdot \mathrm{e}^{-\frac{t}{T_2}} \tag{1.23}$$

with time constant T_2 characterizing the signal decay due to loss of coherence of the precession phase. Locally, T_2 is an indicator of proton mobility. Mobile protons, such as

those in free water, traverse regions of increased and reduced field strength in relatively short time periods, so that opposing effects on the spin phase can partially cancel out, thus slowing signal decay and prolonging T_2. Stationary protons, on the other hand, are subject to the same magnetic environment for extended periods of time and are therefore less likely to experience cancellation of the effect. Regions of low proton mobility are therefore characterized by small T_2 values. T_2 depends on the magnetic field strength of the MR scanner, with higher field strengths leading to shorter T_2. At a given field strength, different types of biological tissue have characteristic T_2 values (e.g., at 3 T: liver – 42 ms, skeletal muscle – 50 ms, white matter – 69 ms, gray matter – 99 ms, and blood – 275 ms [12]).

Inhomogeneity of the static field $\mathbf{B}_0$ is another cause of signal dephasing. These deviations are caused by the magnetic material response of the tissue. The external field can be amplified or attenuated regionally, depending on the local susceptibility distribution inside the object. Interfaces (between organs or between an organ and air or fluid) and iron-rich regions induce abrupt spatial variation of susceptibility and therefore strongly affect the magnetic field. Spatial variation of $\mathbf{B}_0$ leads to position-dependent precession frequencies, which have a similar effect as the aforementioned spin–spin interactions. The decay time constant due to $\mathbf{B}_0$ inhomogeneity is denoted T_i. The compound effect of both dephasing mechanisms is quantified by $T_2^* = \left(\frac{1}{T_2} + \frac{1}{T_\mathrm{i}}\right)^{-1}$, and the corresponding differential equation and its solution are given by

$$\frac{\partial \mathbf{M}_\perp}{\partial t} = -\frac{1}{T_2^*}\mathbf{M}_\perp \tag{1.24}$$

$$\text{and} \quad \mathbf{M}_\perp(t) = \mathbf{M}_\perp(0) \cdot \mathrm{e}^{-\frac{t}{T_2^*}}. \tag{1.25}$$

The decay of transverse magnetization due to dephasing is always faster than the restoration of longitudinal magnetization, $T_2^* < T_2 < T_1$. The effect of the inhomogeneity contribution T_i can be reversed through *spin echoes* (SE), which will be discussed in Section 1.5.1. In that case, the signal decays with the time constant T_2 rather than the shorter T_2^*, yielding a stronger signal and hence better image quality. In NMR spectroscopy, the T_2 or T_2^* decay curve is sampled, and its Fourier transform (a Lorentz curve) is analyzed as the signal of interest.

1.4 Bloch Equations

The precession of the transverse component of magnetization and the relaxation effects are combined in the Bloch equation:

$$\frac{\mathrm{d}\mathbf{M}}{\mathrm{d}t} = \gamma \mathbf{M} \times \mathbf{B} + \frac{1}{T_1}(M_0 - M_\parallel)\hat{\mathbf{z}} - \frac{1}{T_2}\mathbf{M}_\perp, \tag{1.26}$$

where $\mathbf{B}$ is the total magnetic field, which can have contributions in addition to $\mathbf{B}_0$, but it is assumed that its deviation from the z-direction (the direction of $\mathbf{B}_0$) is small.[4] In the

4 Notable other contributions are magnetic field gradients, with a magnitude of typically tens of millitesla, the B_1 field with a strength of tens of microtesla, and the chemical shift, which modulates the precession frequency by approximately 3.5 ppm (parts per million) between fat and water. All these contributions are therefore very small compared to the strength of the static B_0 field of typically 1.5 or 3 T and do not change the direction of $\mathbf{B}$ significantly.

absence of additional fields, that is, when $\mathbf{B} = \mathbf{B}_0$, the solution to the Bloch equation is given by [10]:

$$M_x(t) = \exp\left(-\frac{t}{T_2}\right) \cdot (M_x(0) \cdot \cos(\omega_0 t) + M_y(0) \cdot \sin(\omega_0 t)) \tag{1.27}$$

$$M_y(t) = \exp\left(-\frac{t}{T_2}\right) \cdot (M_y(0) \cdot \cos(\omega_0 t) - M_x(0) \cdot \sin(\omega_0 t)) \tag{1.28}$$

$$M_\parallel(t) = M_\parallel(0) \cdot \exp\left(-\frac{t}{T_1}\right) + M_0 \cdot \left(1 - \exp\left(-\frac{t}{T_1}\right)\right). \tag{1.29}$$

For the transverse components M_x and M_y, this represents a rotation about the z-axis with angular frequency ω_0 and exponentially decaying amplitude. The longitudinal component relaxes from its excited state $M_\parallel(0)$ to the equilibrium value M_0. The three equations, (1.27)–(1.29), can be written equivalently in matrix form as follows:

$$\begin{pmatrix} M_x(t) \\ M_y(t) \\ M_\parallel(t) \end{pmatrix} = \begin{pmatrix} \mathrm{e}^{-t/T_2}\cos(\omega_0 t) & \mathrm{e}^{-t/T_2}\sin(\omega_0 t) & 0 \\ -\mathrm{e}^{-t/T_2}\sin(\omega_0 t) & \mathrm{e}^{-t/T_2}\cos(\omega_0 t) & 0 \\ 0 & 0 & \mathrm{e}^{-t/T_1} \end{pmatrix} \begin{pmatrix} M_x(0) \\ M_y(0) \\ M_\parallel(0) \end{pmatrix} + \begin{pmatrix} 0 \\ 0 \\ M_0(1 - \mathrm{e}^{-t/T_1}) \end{pmatrix}. \tag{1.30}$$

Additional B_1 fields are used to induce magnetization flips, as explained in Section 1.2, usually as pulsed fields with a duration of a few milliseconds. For most imaging applications, it is sufficient to assume the flips to be instantaneous, so that Eqs. (1.27)–(1.29) (or Eq. (1.30)) can be used to describe the situation before and after the pulse, with an abrupt change of M_x, M_y, $M_\parallel$ (and potentially the precession phase) in between.

Maxwell's equations state that time-varying magnetic fields are always accompanied by an electric field, thus forming an electromagnetic field. Due to its frequencies of 63 and 126 MHz on 1.5- and 3-T MR scanners, respectively, a pulsed electromagnetic field is referred to as a *radiofrequency* (RF) pulse.

1.5 Echoes

Thus far, we have seen how RF pulses can be used to flip the magnetization coherently from the z-axis into the xy-plane to generate a measurable MR signal. However, due to relaxation effects, the signal amplitude will decrease exponentially as the transverse magnetization dephases. The signal following immediately after an excitation pulse is called *free induction decay* (*FID*), and its decay constant is T_2^*, the shortest of the three relaxation constants T_1, T_2, and T_2^*. *Spin echoes* and *gradient echoes* are two mechanisms that allow one to modulate and partially recover these signal losses. In the following sections, we will explain the underlying principles.

1.5.1 Spin Echoes

Spin echoes deploy a 180° RF-pulse to reverse the dephasing of the in-plane magnetization after an excitation. The process is illustrated in Figure 1.3.

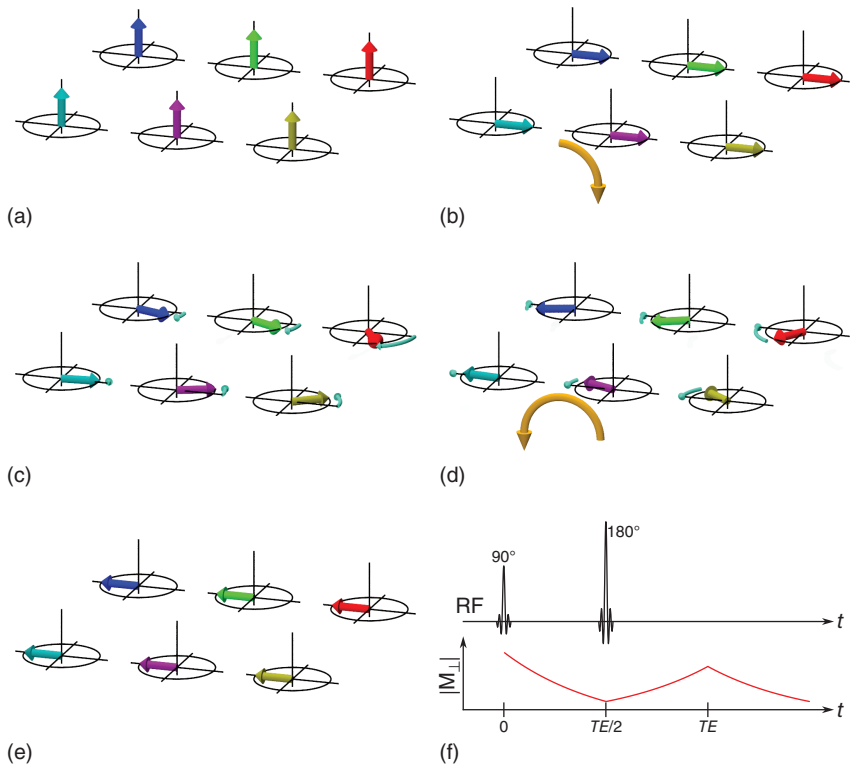

Figure 1.3 Illustration of the spin-echo principle, from the rotating-frame perspective. The arrows correspond to six isochromats at different positions within the imaging plane with different precession frequencies. The direction of the static magnetic field is upward. (a) Equilibrium. (b) Excitation (90° pulse). (c) Free precession. (d) 180° pulse. (e) Echo formation. (f) Timing diagram.

Each arrow in Figure 1.3 represents the magnetization of an isochromat (ensemble of spins with the same precession frequency) at different positions in the imaging plane. The precession frequencies of the isochromats are distinct from one another due to deviations of the magnetic field strength caused by susceptibility effects or B_0 inhomogeneity. Initially, all isochromats are in thermal equilibrium and their magnetic moments are aligned with the magnetic field along the z-axis (Figure 1.3a). An RF pulse is irradiated (shown as a 90° pulse, but arbitrary flip angles are possible) and generates transverse magnetization. Directly after the pulse, the magnetization vectors of all isochromats are in phase (b). The isochromats start to precess about the direction of the magnetic field at their individual precession frequencies $\omega_p(x, y)$, indicated by the length of the circular arrows. After a certain time $t = TE/2$ of free precession, the magnetization vectors have dephased, so that their vector sum $|\mathbf{M}_\perp|$ is smaller than after the initial RF pulse (c). Next, a 180° pulse is deployed, which flips the in-plane magnetization (d). During the next $TE/2$ interval, the isochromats continue to precess freely at their individual precession frequencies $\omega_p(x, y)$. Finally, at time $t = TE$ after the excitation pulse, all isochromats are realigned, so that their magnetization vectors add up to maximum amplitude, causing a peak in the recorded MR signal. TE is referred to as *echo time*.

The refocusing pulse can only reverse the effect of spatially dependent precession frequencies due to magnetic field inhomogeneities. As explained in Section 1.3, interactions between spins lead to longitudinal (T_1) and transverse (T_2) relaxation and cause additional decoherence and hence reduce the magnitude of the transverse magnetization over time. If TE is short compared to T_1, such that T_1 relaxation during signal evolution is negligible (which is a realistic assumption for most pulse sequences), the echo amplitude can be approximated by $|S_0| \propto |\mathbf{M}_\perp(TE)| \approx |\mathbf{M}_\perp(0)| \cdot \exp\,(-TE/T_2)$.

1.5.2 Gradient Echoes

Gradient echoes use a pair of dephaser–rephaser gradients rather than a refocusing pulse to generate an MRI echo signal. The working principle is illustrated in Figure 1.4. As in the case of a spin echo, the equilibrium longitudinal magnetization (a) is fully or partially flipped into the transverse plane by an RF pulse of arbitrary flip angle (b). Next, a dephasing gradient (see Section 1.6.1) is applied along the readout axis (indicated by the purple cone), imposing precession frequency dispersion along that axis (c)–(d). The vector sum $|\mathbf{M}_\perp|$ of the precessing magnetization thus decreases. Eventually, the dephasing gradient polarity is reversed (e), indicated by the changed color of the cone. For every isochromat, the amplitude of the gradient-induced field strength modulation is constant, but the sign changes. Spins that initially experience a strong positive field offset due to the dephaser gradient subsequently experience a strong negative field offset. This affects the local precession frequency (in the rotating frame) in the same way; rapidly precessing spins continue to precess rapidly, but the precession direction is inverted. Finally, the rephasing gradient eliminates the effect of the dephasing gradient (at the instance for which the area under the rephaser gradient waveform is equal to the area under the dephaser) and $|\mathbf{M}_\perp|$ is maximized.

Spatial modulation of the precession frequency due to B_0 field inhomogeneity was neglected in Figure 1.4. However, this introduces an additional contribution to spin dephasing and cannot be compensated for by the rephasing gradient. Therefore, in contrast to a spin echo sequence, where decay of the echo amplitude is primarily governed by T_2, the gradient echo amplitude reduces as $|\mathbf{M}_\perp(TE)| = |\mathbf{M}_\perp(0)| \cdot \exp(-TE/T_2^*)$, with $T_2^* < T_2$ (see Section 1.3). For a fixed TE, the gradient echo will thus have lower signal amplitude (and hence lower signal-to-noise ratio) than a spin echo.

1.6 Magnetic Resonance Imaging

The previous sections have described how the NMR effect can be used to generate and manipulate a signal from an ensemble of spins in a magnetic field. This mechanism is sufficient to obtain time-resolved spectra that provide information on relaxation times and chemical compounds contained in a sample. However, the methods introduced so far can only access global properties of an object – we have not yet described how to associate a signal with its position of origin, which is the prerequisite for any imaging modality. In this section, we will therefore explain a process for encoding spatial information in the MR signal and demonstrate how this information can be used to convert a signal into an image. We will then look into different data sampling strategies and finally present some methods for accelerating the imaging process.

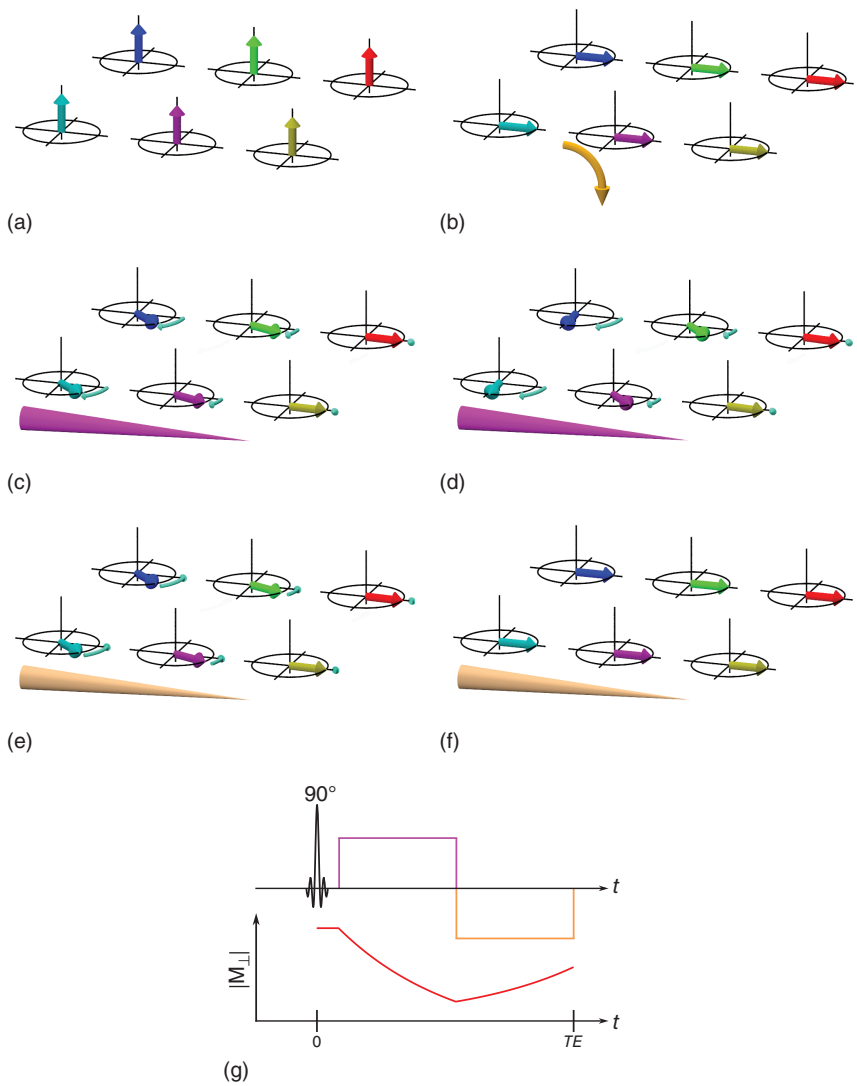

Figure 1.4 Illustration of the gradient echo principle, from the rotating-frame perspective. The arrows correspond to six isochromats with different precession frequencies at different positions within the imaging plane. The direction of the static magnetic field is upward. The cone indicates direction and polarity of the gradient. Further explanations are given in the text. (a) Equilibrium. (b) Excitation (90° pulse). (c) Dephasing gradient. (d) Dephasing gradient. (e) Rephasing gradient. (f) Echo formation. (g) Timing diagram.

1.6.1 Spatial Encoding

Mathematically, an image can be described as a discrete two-dimensional signal, where each pixel can be assigned a unique position in space. In order to generate images from the voltage induced by the precessing transverse magnetization in receive coils, it is necessary to establish a mechanism for spatial encoding of information. The received

signal $S(t)$ can then be interpreted as a superposition of the signals from isochromats (ensembles of spins with the same precession frequency) at different locations, and image reconstruction comprises the decomposition of this compound signal into spatially resolved information.

Three distinct steps are carried out to achieve spatial encoding in three-dimensional space. Each of them requires the application of a *gradient* field. Gradients generate a magnetic field parallel to the z-axis, with the magnitude being linearly dependent on one coordinate:

$$\mathbf{B}(x, y, z) = G_x \, x \cdot \hat{\mathbf{z}} \tag{1.31}$$

for an x-gradient with amplitude G_x, and analogously for y and z. These magnetic fields add to $\mathbf{B_0}$, so that the resultant magnetic field becomes

$$\mathbf{B}(x, y, z) = (B_0 + G_x \, x + G_y \, y + G_z \, z)\hat{\mathbf{z}}. \tag{1.32}$$

Sequential application of three orthogonal gradients leads to three-dimensional spatial encoding of the MRI signal.

1.6.1.1 Slice Selection

As described in Section 1.2, a transverse rotating magnetic field $\mathbf{B}_1$ can be used to tilt magnetization away from its longitudinal equilibrium state and into precessing transverse magnetization. This only works if the rotation frequency ω of $\mathbf{B}_1$ matches the spin precession frequency ω_p. Assuming that a z-gradient field is active while the $\mathbf{B}_1$-pulse is applied, ω_p becomes position-dependent[5]:

$$\omega_p(x, y, z) = \gamma B(x, y, z) = \gamma(B_0 + G_z \cdot z). \tag{1.33}$$

This implies that $\mathbf{B}_1$ can only flip spins at the z-location z_0 for which the resonance condition is fulfilled, that is, where $\omega_p(x, y, z_0) = \omega$. If, instead of being monofrequent, $\mathbf{B}_1$ is designed to be a superposition of precession frequencies with equal amplitudes over a frequency range $(\omega - \delta, \omega + \delta)$, it will flip all spins in the range $(z_0 - \Delta z, z_0 + \Delta z)$ with $\Delta z = \frac{\delta}{\gamma G_z}$. A waveform with uniform amplitude over the interval $(\omega - \delta, \omega + \delta)$, constituting a rectangular pulse in frequency space, corresponds to a sinc[6] in the time domain. Hence, a combination of a *slice-select* gradient and a sinc-shaped $\mathbf{B}_1$-pulse can be used to excite only the spins within a slice of arbitrary orientation and thickness. This process is called *slice selection* (*SS*).

1.6.1.2 Phase Encoding

Phase encoding (*PE*)[7] is the first of two in-plane spatial encoding steps following slice-selective excitation. A phase-encoding gradient, $\mathbf{G}_{\mathrm{PE}}$, is turned on for a limited time T_{PE}. Its direction lies in the imaging plane, perpendicular to the slice-select gradient. This introduces in-plane dispersion of the precession frequency along the direction of the gradient. Let us assume that the magnetization is excited in such a

5 B_1 is about three orders of magnitude smaller than typical gradients, and five to six orders of magnitude smaller than B_0; therefore, its effect on the resonance frequency is negligible.

6 $\mathrm{sinc}(t) = \dfrac{\sin(t)}{t}$.

7 PE in the context of MRI is not related to a technique of the same name used for digital data transmission, also known as Manchester coding.

way that it has zero phase offset in the rotating reference frame after excitation. For simplicity, we will assume further that the imaging plane corresponds to the *xy*-plane (i.e., SS along the *z*-axis) and that the phase-encoding direction coincides with the *y*-axis, $\mathbf{G}_{\mathrm{PE}} = G_{\mathrm{PE}} \cdot \hat{\mathbf{y}}$. After application of the phase-encode gradient pulse, the offset phase is given by

$$\begin{aligned}\phi(\mathbf{r}) &= \mathbf{r} \bullet \left(\gamma \int_0^{T_{\mathrm{PE}}} (\mathbf{B}(x,y,z,t) - \mathbf{B}_0)\, \mathrm{d}t \right) \\ &= \gamma \int_0^{T_{\mathrm{PE}}} \mathbf{r} \bullet (G_{\mathrm{PE}} \cdot \hat{\mathbf{y}})\, \mathrm{d}t \\ &= \gamma \cdot G_{\mathrm{PE}} \cdot y \cdot T_{\mathrm{PE}}. \end{aligned} \tag{1.34}$$

This implies that the *y*-position of a previously excited spin is now encoded in its precession phase.

1.6.1.3 Frequency Encoding

The second in-plane encoding axis is referred to as *frequency encoding* or *readout* (*RO*) direction. After PE, a readout gradient $\mathbf{G}_{\mathrm{RO}}$, perpendicular to the slice selection and phase-encoding directions, is applied while the MR signal is sampled by means of an analog-to-digital converter (ADC) connected to the receive coil(s).[8] If the frequency-encoding axis coincides with the *x*-axis and $t = 0$ denotes the time at which $\mathbf{G}_{\mathrm{RO}}$ is switched on, phase evolution can be expressed as

$$\phi(x,y,z,t) = \gamma(G_{\mathrm{PE}} \cdot y \cdot T_{\mathrm{PE}} + G_{\mathrm{RO}} \cdot x \cdot t). \tag{1.35}$$

The receive coil will "see" this signal (after quadrature detection) as a superposition of all individual signals averaged over space:

$$\tilde{S}(t) = \iiint_{z_0-\Delta z}^{z_0+\Delta z} S_0(x,y,z) \cdot \exp(\mathrm{i}\phi(x,y,z,t))\, \mathrm{d}z\, \mathrm{d}y\, \mathrm{d}x, \tag{1.36}$$

where $S_0(x,y,z)$ is the magnitude of the signal emitted at location $\mathbf{r} = (x,y,z)$. If we use ϕ from Eq. (1.35) and substitute $k_y = \gamma \cdot G_{\mathrm{PE}} \cdot T_{\mathrm{PE}}$ and $k_x(t) = \gamma \cdot G_{\mathrm{RO}} \cdot t$, this can be rewritten as

$$\tilde{S}(k_x,k_y) = \iiint_{z_0-\Delta z}^{z_0+\Delta z} S_0(x,y,z) \cdot \exp(\mathrm{i}(k_x \cdot x + k_y \cdot y))\, \mathrm{d}z\, \mathrm{d}y\, \mathrm{d}x, \tag{1.37}$$

which is the 2D Fourier transform of the in-plane magnetization (averaged over slice thickness $2 \cdot \Delta z$ along the *z*-direction). This means that $S_0(x,y,z)$ can be recovered from the signal $\tilde{S}(k_x,k_y)$ if sufficient data points in *k*-space, spanned by unit vectors $\hat{\mathbf{k}}_x$ and $\hat{\mathbf{k}}_y$, are sampled and then subjected to a discrete inverse 2D Fourier transform. Since k_x is explicitly time-dependent by definition, a line in *k*-space with fixed k_y can be sampled by recording the MR signal over time, while the readout gradient is switched on. k_y is defined by the area under the phase-encoding gradient waveform prior to signal readout, determined by its amplitude G_{PE} and duration T_{PE}. Different lines in

8 Most modern MRI scanners use arrays of receive coils, rather than a single coil. Smaller coils, embedded in a flexible mat or a rigid assembly, can be positioned closer to the object of interest than a single larger coil, enabling increased signal quality. Furthermore, parallel imaging (see Section 2.3.3) requires multiple coils with different spatial sensitivity profiles.

k-space can therefore be acquired sequentially by changing the product $G_{PE} \cdot T_{PE}$. A more elaborate method for sampling an entire k-space with a single excitation will be discussed in Section 2.2.2.

If readout of a k-space line were started immediately after the excitation of a transverse magnetization component, T_2^* relaxation would cause the signal amplitude to drop continuously along that line so that the amplitude at one end of the line would be larger than that at the opposite end. This asymmetry would inevitably cause image artifacts after Fourier transform. One technique to overcome such issues is to refocus the signal so that its amplitude reaches a local maximum at a certain time *TE* after excitation. The local signal maximum is called an *echo*, and the interval *TE* between the excitation and the echo is referred to as *echo time*. If readout is performed symmetrically around the echo, so that the first half of the k-space line is sampled on the rising slope of the signal envelope and the second half on the falling slope, the signal amplitude is distributed symmetrically over the line (see Figure 2.4 for an example).